Dynamics of Tidal Locking Effects in the Formation of Binary Asteroid Systems

Tianrun Wu

Department of Physics

University of Colorado Boulder

Thesis Advisor:

Dr. Hsiang-Wen Hsu, LASP

Committee members:

Prof. Harrison Stalvey, Department of Math

Prof. Michael Ritzwoller, Department of Physics

Prof. Mihaly Horanyi, Department of Physics

Defense Copy

March 20, 2023

Acknowledgement

I am very much indebted to my advisor, Dr. Hsiang-Wen Hsu (Sean), for his invaluable guidance and support to both this thesis and my academic growth. Without his insightful feedback and encouragements, this work would not have been possible.

The starting point of this work was Sean's project on dynamics of dust transport of binary asteroid systems. Sean granted me freedom of dominion on the direction of our project, and my choice of this work deviated from his most comfortable zone of research, but he has demonstrated the enthusiasm to learn and discuss with me to make this work better.

I would also like to thank prof. Tobin Munsat for leading me to research, consulting my bold ideas, and providing countless supports along the way.

I am very lucky to have Sean and Tobin in my undergraduate experience. Their amiable and friendly personalities have truly made working enjoyable and anticipated every day. Their warm and welcoming nature has created a positive and supportive learning environment, whether it was discussing the details of my research or just catching up on life, they have always been approachable and willing to lend an ear. Sean and Tobin's kindness, approachability, and genuine interest in their students' well-being have made them not only valuable advisors but also good mentors and friends.

Once again, I express my deepest gratitude to Sean and Tobin.

Draft version September 5, 2023
Typeset using LaTeX **modern** style in AASTeX631

Spin-Orbit Coupling and Orbital Dynamics in the Formation of Binary Asteroid Systems

Tianrun Wu[1] and Hsiang-Wen Hsu[1,2]

[1] *University of Colorado Boulder, Boulder, CO, USA*
[2] *Laboratory for Atmospheric and Space Physics, Boulder, CO, USA*

ABSTRACT

This theoretical study investigates the spin and orbit interplay of binary asteroid systems during their formation. We focus on the angular momentum content in the rotational fission process and the effects of mass transfer flux onto seeds outside the Roche limit. We also considered the influence of secondaries' rotation on the emergence of chaos and established the upper rotational bound using the planar sphere-spheroid model. Furthermore, we addressed a pivotal gap in the classical secular theory at which the satellite body's semimajor axis ratios approach unity, and found a stable equilibrium separation angle of two satellites of $3\pi/5$, thereby concluding that multiple-seed merger event must invoke chaos. Finally, we proposed a mechanism leading to secondary's rotation reduction from the mass accretion process, acting particularly effective under conditions of substantial mass transfer. Overall, our results provide theoretical supports for the evaluation of inheritance of the orbital and spin attributes of binary asteroid systems in the formation process.

Keywords: Resonances, spin-orbit — Satellites, formation — Asteroids, dynamics — Asteroids, rotation

1. INTRODUCTION

A binary asteroid system (BAS) contains a pair of gravitationally bounded asteroids and is frequently observed in the small asteroid population (constituent asteroids' diameters, $D < 15\,\mathrm{km}$). The larger body in a binary asteroid system is referred as the primary, and the smaller body as the secondary. BASs consist of a significant portion, around 15%, of the total asteroid population in the near-earth, main belt, and the Mars-crossing asteroid populations (Pravec et al. 2016).

Corresponding author: Hsiang-Wen Hsu
Sean.Hsu@lasp.colorado.edu

The Rotational Breakup Theory has been widely accepted to be the formation mechanism of the majority of BASs. It is suggested that a typical BAS is formed when a progenitor asteroid spins so fast that materials on the surface experience no gravity and the asteroid undergoes fission and, from the released materials, a stable two-body configuration could form. Overall, The the Rotational Breakup Theory is in good agreement with exisiting observations data (Walsh et al. 2008).

The present work aims to investigate several foundational principles of the Rotational Breakup Theory. Central to this theory are the torques exerted on asteroids as a consequence of thermal influences and asymmetric reflections, most notably the Yarkovsky–O'Keefe–Radzievskii–Paddack (YORP) effect, discussed subsequently. This effect, originating in the 1950s through the collaboration of Ivan Yarkovsky and Vladmir Radzievskii, revolves around the alteration of small asteroids' rotation rates due to the uneven reflection of solar radiation on their surfaces. Subsequently, Stephen Paddack and John O'Keefe postulated that this effect could give rise to the formation of BASs, a concept later coined as the YORP effect. The YORP effect, aptly referred to as a mechanism for accelerated rotation, drives a small, rotating asteroid to reach the so-called "breakup limit". At the breakup limit, the asteroid spins so fast that materials on the equator of asteroids effectively experience no gravitational force, thus are able to depart from the asteroid to the surroundings. Secondaries could form the launched fragments through gravitation and chaotic processes.

The theory has undergone refinements over time to include a good level of details and demonstrates no major conflict with distribution of binary asteroids' population, spin rate, size, age, and shape, tested by simulations and observational data (Bottke et al. 2006; Walsh and Richardson 2006). A generalized depiction suggests that the YORP effect exerts torque on the surfaces of small bodies, causing their rotation rates to surge to the breakup limit within a span of $10^5 - 10^6$ years (Jacobson and Scheeres 2011). For rubble-pile structured asteroids, characterized by a conglomerate of granular materials, the materials around the equator will drift away at the breakup limit and carry away the extra angular momentum of the asteroid. The materials migrate outward through collisions and gravitational interactions. Once the materials move outside of the Roche limit, larger aggregates are able to form, which will be referred to as seeds hereafter. The system's evolution persists until the seed(s) solidify into a stable configuration, involving possibilities of return, escape, or accretion. Due to the loss of surface material, the primary asteroid undergoes a redistribution until the YORP effect acts to decelerate its rotation. This, in turn, prompts a reversal in the YORP-driven acceleration cycle. A visual representation of the rotational fission process and seed formation, as described above, can be found in Figure 2 of the article by Hyodo and Sugiura (2022).

Dynamical study of BASs is an active field of research and aims to understand the orbital elements and stability of these systems. It is shown that non-Keplerian binary systems can have rich dynamics and complex stability conditions (Scheeres

2009). Non-Keplerian considerations are especially important in BASs for their pervasive close orbits and constituent asteroids' irregular shapes. Spin-orbit dynamics as an important branch has been extensively studied, from resonances to chaos to decoupling mechanics (Murray and Dermott 1999).

Prominently, a large portion of the BASs are synchronous binary asteroids (SBA), whose secondaries are in 1:1 spin-orbit resonance, and close binary asteroid systems are almost unanimously SBA (Ćuk 2007; Pravec et al. 2016). A large population of initially tidally locked binary asteroid is instrumental in explaining the orbital profile of BAS by enabling orbit-altering mechanisms like BYORP and tidal evolution (Jacobson et al. 2013).

While tides, thermal forces, and direct gravitational interactions are routinely invoked as prime candidates for inducing 1:1 spin-orbit resonance within BASs, their individual relative contributions are constrained by data limitations and the intricate interplay of effects. Classical planetary tidal locking models, when applied to BASs, yield timescales on the order of tens of millions of years, while the lifespan of BASs is speculated to be on the same or shorter timescale. This poses a challenge in explaining the large SBA population (Ćuk 2007; Steinberg and Sari 2011). New tidal theories have been proposed for BASs and shorten the classical tidal locking process by around a factor of ten, for example, see (Goldreich and Sari 2009). Chaos in Non-Keplerian dynamics could resonate a secondary with significant mass distribution disparity along its axis of rotation in less than a year, but such secondaries are also unlikely to be Hill stable and eventually escapes the system (Jacobson and Scheeres 2011).

In this work, we focus on the spin-orbit coupling specifically during the formation of BASs, and explore mechanical rotation-altering and orbit-altering processes which are faster-acting and may have a significance in spin-orbit coupling mechanisms. We will also propose a new method in determining the bound and distinguishing chaos of secondary rotations.

2. MASS TRANSFER FLUX AND ORBITAL ECCENTRICITY

In this section, we embark on an exploration of secondary formation and its subsequent orbital evolution during the initial phase of rotational breakup. We elucidate these processes by adopting a straightforward analysis of angular momentum characteristics. This section lays the bedrock upon treatments in the subsequent sections.

We will use the terms material, mass, and grain interchangeably. These terms collectively refer to entities within the system that are distinct from both primary and seed elements. Our analysis is conducted under the assumption of a system exhibiting mild collisional behavior, wherein a substantial population of materials resides within the ring while energetic collisions which cause mass ejection from the system are rare.

2.1. *Mass transfer efficiency*

We introduce the concept of a mass transfer ratio, denoted as σ, which quantifies the proportion of averaged mass transferred to the secondary relative to the total mass that escapes from the primary. This ratio is defined by the integral expression:

$$\sigma = \int_0^\infty \mathrm{d}r \cdot \mathcal{F}(r) \cdot \mathcal{P}(r)\,, \tag{1}$$

Here, the weighting function $\mathcal{F}(r) = \mathrm{Norm}(\mathcal{M}(r) \cdot f(r))$ is introduced, with $\mathcal{M}(r)$ representing the relative mass function for grains of radius r, and $f(r)$ signifying the escape frequency function. The term $\mathcal{P}(r)$ denotes the ratio of granular material transferred to the material that has escaped.

To illustrate the application of this concept, we consider the Didymos - Dimorphos system as a typical example of BASs in the subsequent numerical simulation. Within this simulation, test particles of varying sizes are launched from the primary entity at velocities around the rotational breakup threshold. The integration encompasses gravitational forces, radiation pressure, and solar tides. A radiation pressure efficiency of 0.5 is assumed for all particle sizes.

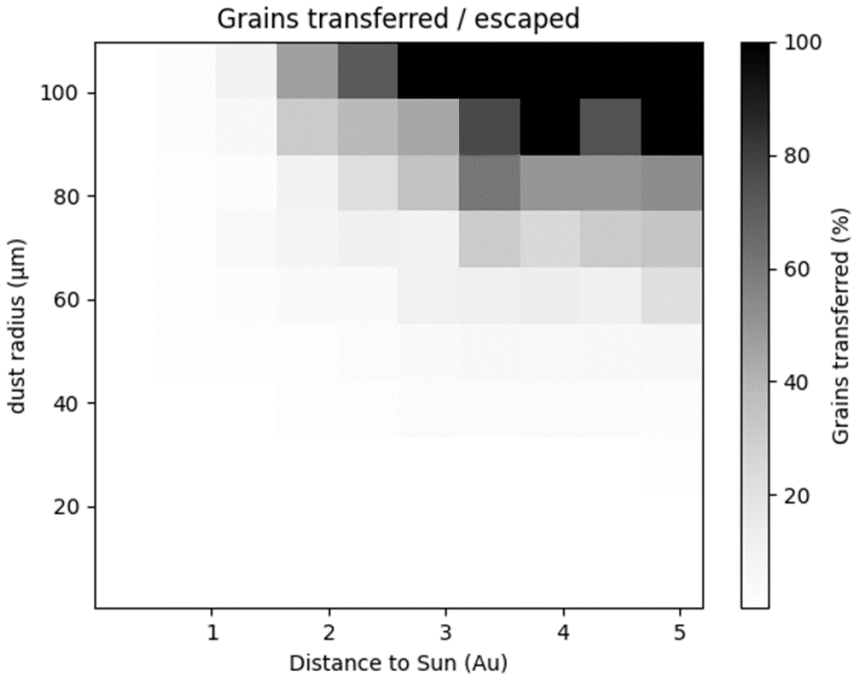

Figure 1. Simulated heat plot of σ as a function of the solar distance and particle size. Extrapolating from the simulation, we expect σ is virtually 1 for particles mm-size and larger regardless of the solar distance. Particles exceeding these dimensions exhibit stable orbits, resulting in a lack of data due to their sustained trajectories over the simulation's allotted time frame of 10 days.

It is shown that in a typical BAS environment, σ for micron-size dusts is mostly from 2% - 70%, and large particles ($r_{\mathrm{grain}} \cdot d_{\mathrm{sun}} \geq 500\,\mu\mathrm{m} \cdot \mathrm{Au}$) hardly escapes the system.

During the formation phase, consider a typical ejected particle size distribution similar to that on asteroid surfaces, which has considerable amount of large boulder, the majority of mass lies in the larger particles. This thereby justifies the assumption of an overall σ value of 1. In the subsequent sections, we will not consider mass loss in the formation phase of BASs and assume all mass escaped from the primary is deposited onto the secondary.

2.2. *Outward migration of rotational fission ejecta*

We now examine the dynamics of materials ejected from the primary. To the first order, a secondary can only form outside Primary's Roche limit. It is thus important to examine if rotational fission ejecta could migrate outward and reach the Roche limit boundary. We consider a system where ejecta particles are produced continuously, generating a collisional disc around the primary. While materials collide and dissipates energy, the total angular momentum remains conserved. Consequently, the average radial distance of fission ejecta remains unchanged while the average orbital eccentricity decreases. With a close-to-unity ejecta mass transfer rate (Sect. 2.1), we focus on the angular momentum of ejecta particles from a collective perspective.

Consider a configuration featuring a spheroidal primary asteroid undergoing rotational fission, whose mass is denoted as M_1, its radius r_1, and an angular velocity ω_1. This primary body undergo fission gives rise to an ejecta ring with a mass of M_2 (which could initially be zero), and this ring orbits at a mean semimajor axis a. By taking the time derivative of the system's angular momentum, given as the sum of orbital and primary body angular momenta, and rearranging the equation, we obtain:

$$\frac{\dot{a}}{2a} = \frac{m r_1^2 \omega_1}{M_1 M_2 \sqrt{\frac{\mathcal{G}a}{M_1+M_2}}} + \frac{m}{M_1} - \frac{m}{M_2}\,, \tag{2}$$

In this expression, $\mathcal{G}$ represents the gravitational constant, $m = -\dot{M}_1 = \dot{M}_2$ denotes the mass transferred from the primary to the secondary over a given time interval, ω_1 stands for the angular velocity of the primary's rotation, and a signifies the semimajor axis of the mutual orbit.

An intriguing insight is gleaned from Eq. 2, as it reveals that a tends towards a state of local equilibrium defined by

$$s\sqrt{\frac{r_1}{a}} = \frac{M_1 - M_2}{M_1 + M_2}\,, \tag{3}$$

where s represents the ratio of ω_1 to the angular velocity corresponding to the rotational breakup limit.

The evolution of the orbital semimajor axis, a, is numerically soluble. For demonstration purpose, we disregard changes in primary's rotation and simulated the orbital migration using the parameters of Didymos to serve as an illustrative case for small,

i.e., BASs. Notably, Eq. 3 is independent of the primary's density, and the appearance of parameters solely in the form of ratios. Thus this demonstration can be extrapolated to a wide array of binary systems.

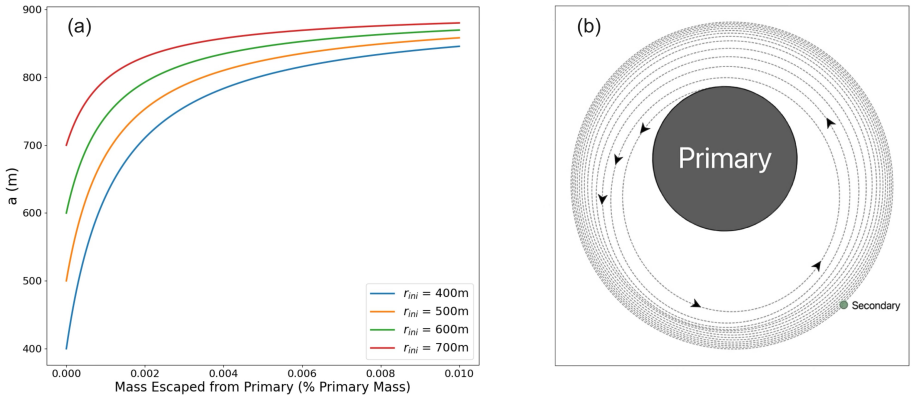

Figure 2. Panel (a) shows rings of different initial radial distance within the Roche limit will migrate outward as the ring absorbs mass ejected by the primary. Parameters of Didymos – Dimorphos system with initial angular speed at 1.1 times the breakup limit were used in simulation. The radius and the Roche limit radius of Didymos is about 380m and 1000m, respectively. Panel (b) shows a sketch of a seed located in the ring migrating outward.

The simulation results are presented in Fig. 1. Evidently, the coupling between angular momenta of primary's rotation and the orbit is sufficient to support the outward motion of ejecta ring. The primary's angular momentum is transferred to the mutual orbit and serves as the driving force behind the movement of materials towards the vicinity of the Roche limit. Our result also shows that, independent of the initial locations, the final orbital radius of the ejecta ring converges to a location approaching the Roche limit.

2.3. *Further evolution of the ejecta ring*

Fission ejecta likely exhibit a broad size distribution , ranging from multi-meter-sized boulders to a multitude of granular entities down to centimeter-scale and smaller. The positioning of these materials within the Roche limit imparts a nuanced quality to the interactions among them. Within this regime, interactions involving the larger boulders can be approximated as elastic collisions, while the smaller granular components primarily engage in inelastic collisions, as the cohesion force becomes more and more important with decreasing grain size. (Blum and Schräpler 2004; Walsh et al. 2022).

Over time, the sequence of elastic collisions involving the boulders leads to the emergence of particular distributions governing both velocity and angular momentum,

akin to the Maxwell-Boltzmann distribution. This phenomenon finds parallels in the field of material kinetics within planetary rings, and readers may find pertinent insights from those studies (e.g. Bodrova et al. 2012).

Resulting from the characteristics of the aforementioned distributions, the possibility rises that a fraction of ejecta particles could acquire sufficient angular momentum, thereby drift beyond the Roche limit's boundary. It is noteworthy that most larger boulders, lacking the requisite angular momentum for egressing the Roche limit, will necessarily undergo an evolutionary trajectory that ultimately leads them fall back toward the primary body.

In accordance with the angular momentum redistribution mechanism that we've proposed, the seeds' angular momentum is not anticipated to significantly exceed the threshold necessary for their escape from the Roche limit. This expectation is grounded in the observation that the likelihood of attaining excessive angular momentum diminishes considerably as the distribution approaches its extreme values. Concurrently, in instances where seeds do acquire augmented angular momentum due to collision events, a portion of their orbital path may still traverse within the Roche limit due to the presence of nonzero eccentricity. Under such circumstances, near the periapsis of their orbits, these seeds will undergo reentry into the interior of the Roche limit. During this process, energy and angular momentum will be transferred back to the materials within the Roche limit, culminating in the circularization of the orbit. Consequently, the final state of the seed's orbit will position itself merely outside the Roche limit, thus engendering an anticipation of low eccentricity.

3. ROTATIONAL BOUND AND ONSET OF CHAOS

In this section, our investigation delves into the constraints governing the rotation of seeds, guided by considerations of the onset of chaos. Drawing inspiration from the work on full two-body dynamics by Scheeres (2002), we adopt an approach wherein the N bodies are partitioned into two substantial aggregates, denoted as M_p and M_s. These aggregates, characterized by both translational and rotational motion confined to a plane, allow us to capitalize on the holonomic constraints inherent to two-body problems. For simplicity, we assume that the mutual orbit is positioned on a circular torus, a choice that reduces complexity in the resultant equations. We will show that the results are valid and applicable even if the orbit has non-zero eccentricity.

The rotational inertia I, kinetic energy T, and angular momentum L for a many body system are denoted respectively as follows:

$$I = \sum_{i=1}^{N} m_i \mathbf{r}_i^2 \tag{4}$$

$$T = \frac{1}{2} \sum_{i=1}^{N} m_i \dot{\mathbf{r}}_i^2 \tag{5}$$

$$L = \sum_{i=1}^{N} m_i \mathbf{r}_i \times \dot{\mathbf{r}}_i \,. \tag{6}$$

We'll draw upon two well-established results from N-body motion, namely the Lagrange–Jacobi identity (Dmitrašinović 2020)

$$\ddot{I} = 4T - 2\sum_{i=1}^{N} \mathbf{r}_i \cdot \nabla U(\mathbf{r}_i) = 4T + 2U \tag{7}$$

and the Sundman's inequality (Muller 1986)

$$2IT \geq \frac{\dot{I}^2}{4} + L^2 \,. \tag{8}$$

Note that, these results maintain their validity even in the presence of non-gravitational forces. This justifies our categorization of the N bodies into two granular aggregates.

Given our assumption of two-body granular aggregates, Eq. 4 can be expressed as follows:

$$\begin{aligned} I &= \sum_{i=1}^{N} m_i \mathbf{r}_i^2 = \mu \mathbf{r}^2 + \sum_{i \in I_1} m_i \mathbf{r}_{1,i}^2 + \sum_{i \in I_2} m_i \mathbf{r}_{2,i}^2 \\ &= \mu \mathbf{r}^2 + \frac{1}{2}\mathrm{Tr}[\mathbf{I}_1] + \frac{1}{2}\mathrm{Tr}[\mathbf{I}_2] \,. \end{aligned} \tag{9}$$

Neglecting the deformation of the two bodies, from Eq. 9,

$$\dot{I}(t) = 2\mu \mathbf{r} \cdot \frac{\partial r}{\partial t} \tag{10}$$

$$\ddot{I}(t) = 2\mu \left(\frac{\partial \mathbf{r}}{\partial t}\right)^2 + 2\mu \mathbf{r} \cdot \frac{\partial^2 \mathbf{r}}{\partial t^2} \,, \tag{11}$$

where $\mu = M_p M_s/(M_p + M_s)$ is the reduced mass of the two bodies.

Aligned with our observational findings, we posit that the primary possesses an axisymmetric form (equivalent to its center of mass in planar two-body problems), while the secondary assumes an irregular elongated shape (Ćuk 2007). $\mathbf{r}$ is the displacement from the effective point mass of the primary to that of the secondary. Notably, an effective point of mass refers to a point where the experienced gradient of the gravitational potential field matches that of a calculated body. In Keplerian (spherical) two-body problems,the effective point of mass coincides with the center of mass. However, in the context of non-Keplerian dynamics as how our problem is setup, deviations arise, necessitating the consideration of a point mass slightly offset from the center of mass.

To facilitate our analysis, we introduce $r = r_0 + \tilde{r}$, where r_0 is the distance between the two bodies' center of masses. Compared to $\tilde{r}$, r_0 variates negligibly as movements in the center of mass requires considerable amount of energy exchange. Therefore, we will treat r_0 as invariant, and $\tilde{r}$ as the periodic part. The periodicity is presumably

predominantly caused by the rotation of secondary. Apply to Eqs. 7, 10, 11 and linearize:

$$\dot{I}(t) = 2\mu \mathbf{r}_0 \cdot \frac{\partial \tilde{r}}{\partial t} \tag{12}$$

$$\begin{aligned} \ddot{I}(t) &= 2\mu \left(\frac{\partial \mathbf{r}_0}{\partial t} + \frac{\partial \tilde{r}}{\partial t} \right)^2 + 2\mu \mathbf{r}_0 \cdot \left(\frac{\partial^2 \mathbf{r}_0}{\partial t^2} + \frac{\partial^2 \tilde{\mathbf{r}}}{\partial t^2} \right) \\ &= 2\mu \left(\left(\frac{\partial \tilde{r}}{\partial t} \right)^2 + v_{\text{orb}} \frac{\partial \tilde{r}}{\partial t} + r_0 \frac{\partial^2 \tilde{r}}{\partial t^2} \right) \end{aligned} \tag{13}$$

$$\begin{aligned} T = \frac{\ddot{I} - 2U}{4} = \frac{\mu}{2} &\left(\left(\frac{\partial \tilde{r}}{\partial t} \right)^2 + v_{\text{orb}} \frac{\partial \tilde{r}}{\partial t} + r_0 \frac{\partial^2 \tilde{r}}{\partial t^2} \right) \\ &- (U_{\text{orb}} + U_2) , \end{aligned} \tag{14}$$

where v_{orb} is the circular orbital velocity at r_0, U_{orb} is the gravitational potential energy of orbital coupling, and U_2 is the gravitational potential energy contained by the secondary.

We adopt the simplification of treating the primary as a point mass, which allows us to eliminate both I_1 and its corresponding rotational angular momentum contribution from Eq. 8. Additionally, considering the secondary's rotational angular momentum contribution to be insignificantly small compared to the orbit, we can prudently exclude it without violating any constraints.

Employing these simplifications in Eq. 8, we arrive at

$$\left(\mu r_0^2 + \frac{1}{2} \text{Tr}[I_2] \right) T \geq \left(\mu r_0 \cdot \frac{\partial \tilde{r}}{\partial t} \right)^2 + L^2 \tag{15}$$

Moreover, we introduce substitutions for I_2 and U_2 by using

$$\begin{cases} l = \dfrac{I}{\mu r_0^2} \\ k = \dfrac{U}{U_{\text{orb}}} . \end{cases} \tag{16}$$

Insert Eq. 16 into Eq. 15 yields

$$\frac{2lT}{\mu} \geq \left(\frac{\partial \tilde{r}}{\partial t} \right)^2 + \frac{L^2}{\mu^2 r_0^2} . \tag{17}$$

Substituting Eq. 14 into Eq. 17 and rearranging, we obtain

$$\begin{aligned} v_{\text{orb}} \frac{\partial \tilde{r}}{\partial t} + r_0 \frac{\partial^2 \tilde{r}}{\partial t^2} &\geq \left(\frac{v_{\text{orb}}^2}{\alpha} + \frac{k U_{\text{orb}}}{\mu} \right) \\ &= \left(\frac{1}{l} - k \right) v_{\text{orb}}^2 . \end{aligned} \tag{18}$$

Given our assumption that $\tilde{r}$ exhibits periodic motion, we can deduce

$$\left| v_{\text{orb}} \frac{\partial \tilde{r}}{\partial t} + r_0 \frac{\partial^2 \tilde{r}}{\partial t^2} \right| \leq \left(k - \frac{1}{l} \right) v_{\text{orb}}^2 , \tag{19}$$

This expression can alternatively be represented as

$$\left|\frac{\partial\tilde{r}}{\partial t}\right| = \omega\Delta\tilde{r} \leq \left(k - \frac{1}{l}\right)\frac{r_0\omega_{\rm orb}^2}{\omega_{\rm orb}+\omega}\,, \tag{20}$$

where $\omega_{\rm orb}$ is the circular angular velocity at orbital radius r_0. The soluation of Eq. 20 is

$$\omega \leq \frac{1}{2}\left(\sqrt{1+\left(k-\frac{1}{l}\right)\frac{4r_0}{\Delta\tilde{r}}}-1\right)\omega_{\rm orb}\,. \tag{21}$$

To gauge the extent of variation in $\tilde{r}$ and express ω in a more practical manner, we resort to approximating the secondary entity as an oblate spheroid characterized by a semi-major axis of a_s, a semi-minor axis of b_s, and an ellipticity $e = \sqrt{1-b_s^2/a_s^2}$. Should the need arise to establish a more accurate mass distribution, such a goal can be achieved by modifying the gravitational potential energy through the incorporation of MacCullagh's formula ([Internet] 2003).

The gravitational potential energy outside of an oblate spheroid is given by (Hofmeister et al. 2018).

$$\Phi \approx -\frac{\mathcal{G}M_2}{r_0}\left(1-\frac{3\sin^2\theta-1}{10}\left(\frac{a_s e}{r_0}\right)^2\right)\,, \tag{22}$$

where θ represents the orientation angle from the spheroid's semiminor axis. The maximum variation in $\tilde{r}$ can be calculated from the extremes of Φ, and keep it only to the first non-zero term

$$\Delta\tilde{r} = \frac{9}{20}a_s^2e^2\,. \tag{23}$$

Let's now re-examine l and k. The moment of inertia of spheroid in its principal axes is

$$I_2 = \frac{M}{5}\begin{pmatrix} 2b_s^2 & 0 & 0 \\ 0 & a_s^2+b_s^2 & 0 \\ 0 & 0 & a_s^2+b_s^2 \end{pmatrix}\,; \tag{24}$$

and the gravitational binding energy of a spheroid is (Scheeres 2004)

$$\begin{aligned} U_2 &= -\frac{3}{5}\frac{\mathcal{G}M_2^2}{a_s b_s}\left(a_s^2+b_s^2-\frac{2b_s^3}{\sqrt{a_s^2-b_s^2}}\arctan\left(\sqrt{\frac{a_s-b_s}{a_s+b_s}}\right)\right) \\ &\approx -\frac{3}{5}\mathcal{G}M_2^2\left(\frac{1}{a_s}-\frac{5e^2}{6a_s}\right)\,. \end{aligned} \tag{25}$$

With Eqs. 16, 24 and 25, l and k are transformed to

$$\begin{cases} l = 1+\dfrac{3-2e^2}{5}\left(1+\dfrac{M_2}{M_1}\right)\left(\dfrac{a_s}{r_0}\right)^2 \\ k = 1+\dfrac{3}{5}\dfrac{M_2}{M_1}\dfrac{r_0}{a_s}-\dfrac{1}{2}\dfrac{M_2}{M_1}\dfrac{r_0e^2}{a_s} \end{cases}\,. \tag{26}$$

By combining Eqs. 26 and 21, the rotational bound for a given spheroidal secondary on a circular orbit is formulated as

$$\omega \leq \frac{1}{2}\left(\sqrt{\frac{48-88e^2}{9e^2}\left(\frac{r_0}{r_1}\right)^3+\frac{48-23e^2}{9e^2}}-1\right)\omega_{\rm orb}\,. \tag{27}$$

Eq. 27 and Fig. 3 shows that, near the Roche limit, a typical elongated seed's rotation period is capped at around 7 times that of the orbital period (Johnston 2022). In other words, Eq. 27 provides a rotation period upper limit for a secondary form slowly from materials ejected from rotational breakup.

This rotational limitation becomes even more pronounced when the mutual orbit deviates from circularity and possesses non-zero eccentricity. The rationale for this enhancement can be understood by examining the constituents of Eq. 8. Notably, the left-hand side is roughly proportional to r, the radial distance, while the right-hand side remains invariant to the first order of r. Among orbits sharing the same semimajor axis, circular orbit results in the largest r values throughout their trajectory. Thus, any violation of the inequality in Eq. 27 implies that either the seed reshapes and reduces its elongation, or the orbital motion transitions into a realm of chaos. While the fractal of chaotic orbital motion cannot be determined from Eq. 27 alone, we show that the dynamical relationship between rotation, shape, and orbital characteristics offers a simple and viable boarder for initiation of chaos in close binary systems.

4. SECULAR THEORY FOR SEED MERGER

In the case that there's more than one seed, the dynamical evolution leading such system to become BASs could be drastically different. Although double-satellite asteroid systems do exist, their prevalence significantly lags behind that of BASs. Therefore, our focus pertains to the merger of seeds. We are specifically concerned with the merger of two seeds, as it represents a probable evolutionary path and captures the fundamental dynamics of multiple-seeds interactions, yet its dynamics remain to be addressed by classical secular theory.

Prior to the coalesce of the two seeds, their orbital semimajor axes (denoted a and a') gradually converge. Classical secular theory encounters a fundamental obstacle in this context, as the Laplace coefficients diverge to infinity when the ratio of semimajor axes approaches unity. We circumvent this divergence by directly substituting the disturbing function into the equations of motion.

The equations governing planer motion of a single satellite body in polar coordinates is given by (Brouwer and Clemence 2014, chap. 2)

$$\ddot{r}-r\dot{\phi}^2+\frac{\partial V}{\partial r}=0 \tag{28}$$

$$r^2\dot{\phi}=G\,, \tag{29}$$

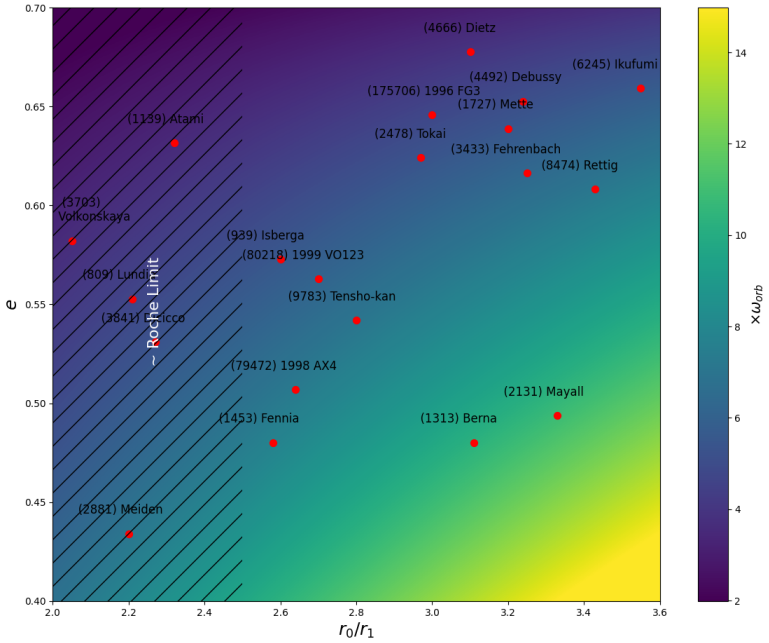

Figure 3. Rotational bound of seeds (ω_2) on circular orbits. Actual binary asteroid systems' data are also plotted. At the Roche limit, the rotational cap for most secondaries is below sevenfold the orbital rotation. As secondaries migrate further outward, the bound loosens significantly.

where ϕ is the true anomaly of the body. For near circular orbits, $G \approx a^2 n$, where n is the mean motion.

In the presence of perturbations, we introduce ρ and γ as small quantities characterizing the proportion of deviations from the unperturbed orbit, and modify the right-hand side of Eq. 29 as $G(1+\gamma)$ and write $r = a(1+\rho)$.

Additionally, we expand r in terms of δr as $r = a + \delta r$, and the potential V as $V = V_{\text{prim}} + \mathcal{R}$. Where δr and $\mathcal{R}$ are deviations from the unperturbed orbit. δr relates to ρ by $\rho = \delta r/a$.

Incorporating these modifications, Eqs. 28 and 29 transform to

$$(\ddot{a + \delta r}) - (a + \delta r)\dot{\phi}^2 + \frac{\partial V_{\text{prim}} + \mathcal{R}}{\partial r} = 0 \tag{30}$$

$$(a + \delta r)^2 \dot{\phi} = a^2 n(1+\gamma)\,. \tag{31}$$

Substituting Eq. 31 into 30, we obtain

$$(\ddot{a + \delta r}) - \frac{a^4 n^2 (1+\gamma)^2}{(a+\delta r)^3} + \frac{\partial (V_{\text{prim}} + \mathcal{R})}{\partial r} = 0\,. \tag{32}$$

By separating the perturbation terms according to order, we have

$$\ddot{\delta r}_{(1)} + 2an^2\gamma_{(1)} + 3n^2\delta r_{(1)} + \left(\frac{\partial \mathcal{R}}{\partial r}\right)_{(1)} = 0 \tag{33}$$

$$\ddot{\delta r}_{(2)} + 2an^2\gamma_{(2)} + an^2\gamma_{(1)}^2 + 3n^2\delta r_{(2)} - 6n^2\delta r_{(1)}\gamma_{(1)} + \left(\frac{\partial \mathcal{R}}{\partial r}\right)_{(2)} = 0\,. \tag{34}$$

Continuing with our analysis and considering $\partial\mathcal{R}/\partial r$ under the assumption of $a = a'$, we will investigate the behavior of δr up to the second order, $\delta r_{(1)} + \delta r_{(2)}$. For this purpose, it is appropriate to designate the perturber's radial distance as $r' = a' + \delta r'_{(1)}$. We will ensure that the subsequent quantities are maintained to relevant orders. Note that we use primed quantities to signify the perturbing body, and interchanging primed and unprimed variables in expressions allows the conversion of derived quantities between perturbing and perturbed bodies.

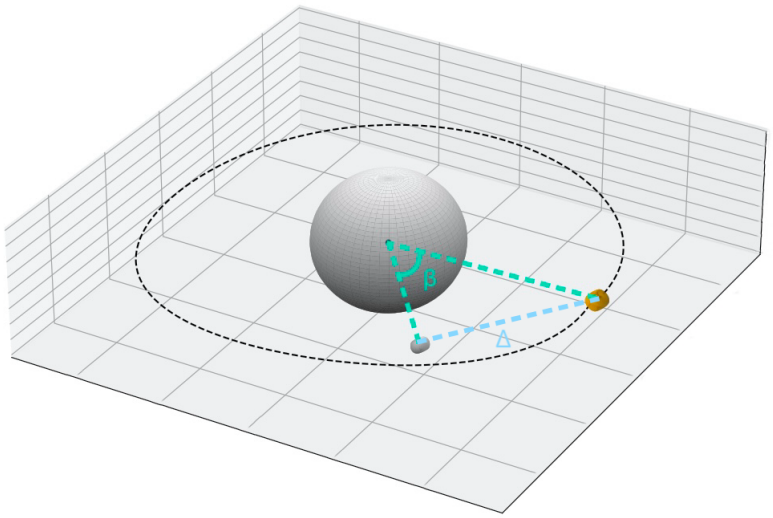

Figure 4. A sketch of two seeds on similar circular orbits and subject to mutual perturbations. The mutual distance Δ and mutual angle β are labeled on the graph.

Denote $\alpha = r/r' \approx 1 + \rho - \rho'$, Δ the mutual distance between the two seeds, and β the mutual angle of the two seeds, as shown in Fig. 4. For $0 < \beta < 2\pi$, we have

$$\begin{aligned} \frac{r'^3}{\Delta^3} &= (1 + \alpha^2 - 2\alpha\cos\beta)^{-\frac{3}{2}} \\ &\approx \frac{2 - 3(\rho - \rho')}{16}\csc^3\frac{\beta}{2}\,. \end{aligned} \tag{35}$$

The disturbing function for this configuration is

$$\mathcal{R} = \mathcal{G}m'\left(\frac{1}{\Delta} - \frac{\mathbf{r}\cdot\mathbf{r}'}{r'^3}\right)\,. \tag{36}$$

Taking the partial derivative of $\mathcal{R}$ with respect to r gives

$$\frac{\partial\mathcal{R}}{\partial r} = \frac{\mathcal{G}m'}{a'^2(1+\rho')^2}\left((\cos\beta - \alpha)\left(\frac{r'}{\Delta}\right)^3 - \cos\beta\right)\,. \tag{37}$$

Expanding Eq. 37 in terms of ρ and ρ' by order, we have

$$\left(\frac{\partial \mathcal{R}}{\partial r}\right)_{(1)} = -\frac{\mathcal{G}m'}{a'^2}\left(\cos\beta + \frac{1}{4}\csc\frac{\beta}{2}\right) \tag{38}$$

$$\begin{aligned}\left(\frac{\partial \mathcal{R}}{\partial r}\right)_{(2)} = \frac{\mathcal{G}m'}{a'^2}\Bigg(&\rho\left(\frac{1-3\cos\beta}{8}\right)\csc\frac{\beta}{2} \\ &+\rho'\left(\frac{7\cos\beta+3}{64}\right)\csc\frac{\beta}{2}\Bigg)\,.\end{aligned} \tag{39}$$

Combining Eqs. 33 and 38, we obtain

$$\begin{aligned}\delta r_{(1)} = c_1\sin(\sqrt{3}nt + c_2) \\ &- \frac{\sin(\sqrt{3}nt)}{\sqrt{3}n}\int_1^t \mathrm{d}\tau\cdot\cos(\sqrt{3}n\tau)f(\tau) \\ &+ \frac{\cos(\sqrt{3}nt)}{\sqrt{3}n}\int_1^t \mathrm{d}\tau\cdot\sin(\sqrt{3}n\tau)f(\tau)\,,\end{aligned} \tag{40}$$

with

$$f(t) = \left(\frac{\partial \mathcal{R}}{\partial r}\right)_{(1)} + 2an^2\gamma_{(1)}\,. \tag{41}$$

We disregarded the influence of the perturbative parts of the orbit on β to ensure the system can be solved in general forms. Before continuing to solve the second order of δr, simplification of Eq. 34 is needed. Denote the deviation of the true anomaly of the perturbed body from the unperturbed configuration as $\mathcal{E} = \phi - \lambda$, where $\lambda = nt + \lambda_0$ is the mean longitude, equivalent to the true anomaly of the circular orbit. Taking the derivative of $\mathcal{E}$ with respect to λ gives

$$\frac{\partial \mathcal{E}}{\partial \lambda} = \frac{1+\gamma}{(1+\rho)^2} - 1\,. \tag{42}$$

Expand Eq. 42 in terms of γ and ρ, we get

$$\frac{\partial \mathcal{E}_{(1)}}{\partial \lambda} = \gamma_{(1)} - \frac{2\delta r_{(1)}}{a}\,. \tag{43}$$

Integrating Eq. 43 with respect to λ yields

$$\mathcal{E}_{(1)} = (2an^2+1)\gamma_{(1)}\lambda - \frac{c_1}{\sqrt{3}}\cos(\sqrt{3}nt + c_2) + \text{Const.}\,. \tag{44}$$

To avoid $\mathcal{E}$ dependent on λ, $\gamma_{(1)}$ must be zero. $\mathcal{E}_{(2)}$ can be calculated with similar arguments if needed.

By applying this result, Eq. 34 simplifies to

$$\ddot{\delta r}_{(2)} + 2an^2\gamma_{(2)} + 3n^2\delta r_{(2)} + \left(\frac{\partial \mathcal{R}}{\partial r}\right)_{(2)} = 0\,. \tag{45}$$

Combining Eqs. 45 and 39, we obtain the solution for $\delta r_{(2)}$:

$$\begin{aligned}\delta r_{(2)} = c_3 \sin(\sqrt{3}nt + c_4) \\ - \frac{\sin(\sqrt{3}nt)}{\sqrt{3}n} \int_1^t \mathrm{d}\tau \cdot \cos(\sqrt{3}n\tau) g(\tau) \\ + \frac{\cos(\sqrt{3}nt)}{\sqrt{3}n} \int_1^t \mathrm{d}\tau \cdot \sin(\sqrt{3}n\tau) g(\tau)\,,\end{aligned} \tag{46}$$

with

$$g(t) = \left(\frac{\partial \mathcal{R}}{\partial r}\right)_{(2)} + 2an^2\gamma_{(2)}\,. \tag{47}$$

As the seeds approach to merge, i.e., $\beta \to 0$, both $f(t)$ and $g(t)$ diverge to infinity, and δr also approaches infinity, a state that contradicts the near-circular orbit assumption. Consequently, the merger of seeds in a non-chaotic manner is unfeasible. In cases where seeds merge amidst chaotic dynamics, the resultant merged secondary is unlikely to align in a spin-orbit resonance configuration, nor will its orbit be circular.

Examining Eq. 40, we find first-order stable "equilibrium points"at $\beta = 3\pi/5$ and $\beta = 7\pi/5$, corresponding to instances where $f(t) = 0$. Near these points, $\delta r_{(1)}$ converges to its first sinusoidal term over time, and the stability can be examined by denoting the last two terms of $\delta r_{(1)}$ as $h(t)$, and take the time derivative

$$\begin{aligned}\dot{h}(t) = -\cos(\sqrt{3}nt) \int_1^t \mathrm{d}\tau \cdot \cos(\sqrt{3}n\tau) f(\tau) \\ + \sin(\sqrt{3}nt) \int_1^t \mathrm{d}\tau \cdot \sin(\sqrt{3}n\tau) f(\tau)\,,\end{aligned} \tag{48}$$

which always has the opposite sign as $h(t)$.

These results suggest that, when these two seeds come close to each other in near-circular orbits, the mutual perturbation makes each of their orbital radii oscillate, and their angular separation will approach $3\pi/5$ instead of 0. We conclude that if multiple seed accretion indeed occur, its process must be chaotic and will not lead to a configuration at which a secondary is close to tidal locked, and other spin-orbit dynamics will dominate the final rotation of the merged secondary.

5. SEED ROTATION REDUCTION

In preceding sections, we have scrutinized the intricacies of the spin and orbital dynamics in the early phase of rotational breakup. We investigated the migration and formation of seeds, and developed criteria for seeds to form into low-eccentric orbits with low spin. Now, we shift our focus to the later phase of BAS formation, where a solitary secondary has formed beyond the Roche limit. Within this stage, particle kinetics distribution attains an equilibrium state. Notably, larger particles, on average, exhibit lower angular momentum per unit mass. This phenomenon stems from the secondary's need to carry away a substantial amount of angular momentum to escape the Roche limit.

At this advanced stage, the secondary primarily interacts with smaller particles. This interaction is driven by two factors: firstly, the greater prevalence of smaller particles in the outer ring and their sensitivity to the secondary's gravitational influence, and secondly, insights gleaned from both the classical secular theory and section 4, which affirm that mutual perturbations among larger bodies do not substantially alter orbital semimajor axes and eccentricities.

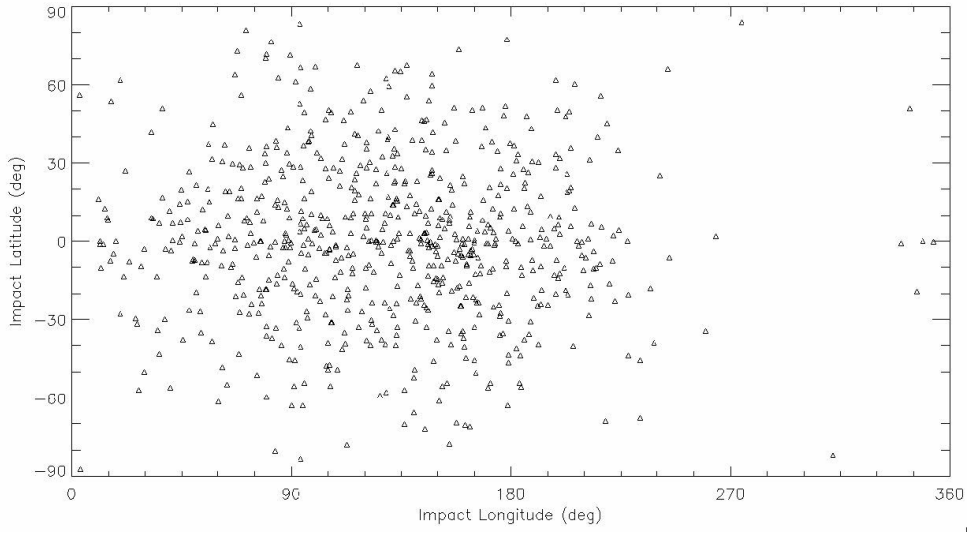

Figure 5. Simulation shows particles mostly impact the leading side of the seed, consistent with the angular momentum argument above.

Given the secondary's location beyond the Roche limit, and considering that accreted granular materials predominantly occupy lower orbits within or around the Roche limit, the secondary contains a comparatively higher angular momentum per unit mass than the ring. As a consequence, the deposition of mass onto the seed predominantly occurs on its leading side, symmetrical in latitude (Fig. 5). Should the seed's rotational angular speed surpass the orbital angular speed, a transfer of angular momentum occurs from the seed to the impacting mass and experiences a consistently non-zero torque. This torque counteracts the seed's rotation, inducing a reduction in its rotational angular speed, as depicted in Fig. 6.

A numerical simulation is carried out to demonstrate the proposed scenario. In the simulation, the rotation of the secondary is randomly selected after each impact event, spanning from 0 to 5 times the orbital angular velocity. The simulation tracks the impact positions of particles on the secondary and calculates the torque per unit impacting mass for each impact event. This information is then utilized to generate a torque profile comprising 500 data points with a dependence on primary's rotation.

Then, we tracked the rotation alteration of a secondary originally rotating five times faster than the orbital rotation. Impacting masses are randomly selected based on a normal distribution of impactor size, centered at 0 m with a standard deviation of 1 m, and corresponding torques are drawn from the generated torque profile. The

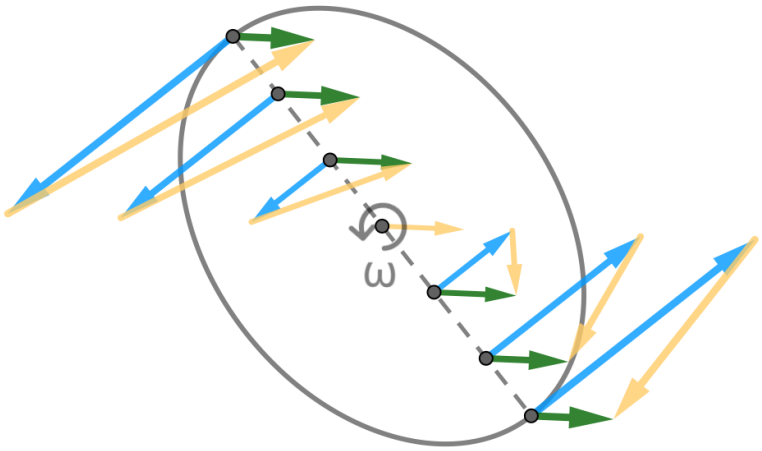

Figure 6. Blue arrows are linear velocity vectors of the seed, green arrows are velocity vectors of incoming masses viewed in the co-rotating frame. Yellow arrows are the velocity vectors of incoming masses viewed in the secondary's rotating frame. It can be seen that a non-zero averaged torque created by the masses counters the rotation of the secondary in the co-rotating frame.

result in Fig. 7 shows that the secondary's rotation rapidly decreases, converging towards a state close to resonance.

6. CONCLUSION

The goal of this work is to understand the interplay of spin and orbital dynamics during the formation of binary asteroid systems, within the framework of the rotational breakup theory. This is motivated by the contrast between the observed predominance of tidal-locking binary asteroid systems and the lengthy processing timescales required to reach 1:1 spin-orbit resonance from arbitrary initial conditions. Our investigation commences with an exploration of how the process of angular momentum transfer influences the evolution of seeds' orbits, driving them towards the vicinity of the Roche limit during the initial stage of rotational breakup. We proceed to investigate the emergence of chaos prompted by the secondary's rotation and establish a rotational bound applicable to planar sphere-spheroid binary systems. This bound is constructed by drawing upon relevant equations and inequality in many body kinetics on simplifications based on non-chaotic configurations.

Significantly, built upon the classical planetary perturbing theory, our results offer new insights as the satellite bodies' orbital semimajor axis ratio approaches unity. We explored the possibility of secondary pertaining to a low rotation rate and low eccentric orbit from the accretion of slowly approaching seeds. We concluded that this possibility is slim, as under mutual perturbations, seeds' radial distance will engage in

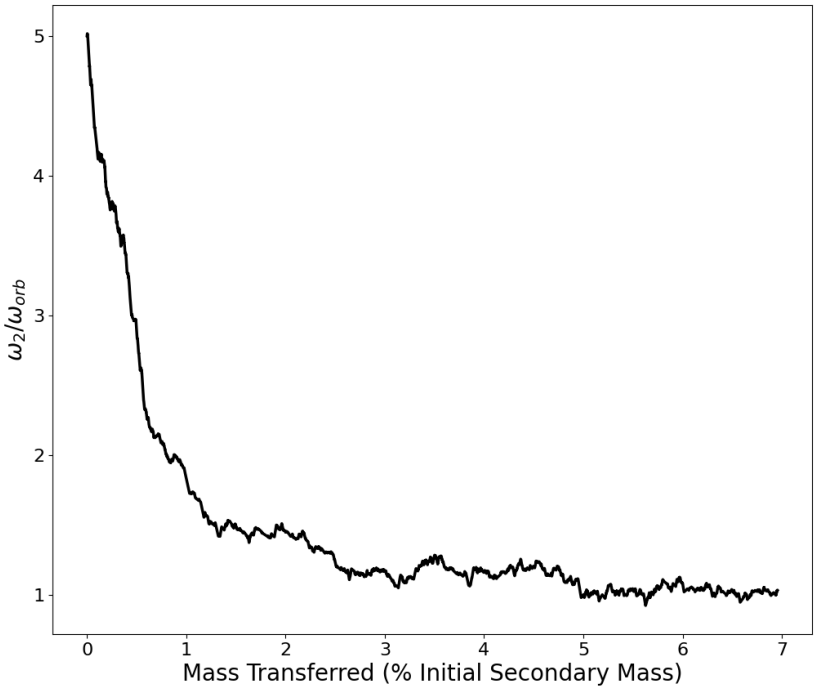

Figure 7. Simulated secondary accreting mass from the ejecta particles. The accretion torque rapidly decreases secondary's rotation to near resonance. The secondary is assumed with a radius 10 m, density 2 g/cm^3, and a circular orbit with a radius of 1000 m.

oscillatory modes and their mutual angle will converge towards $3\pi/5$. The occurrence of a merger event necessarily invokes chaos and the resultant merged entity's orbit and spin would be arbitrarily configured, inconsistent of tidally locked secondary in most BASs.

Our final proposition centers on an mechanical mechanism driving rotation alterations during the concluding stages of BAS formation. This process hinges on the difference in angular momentum between the secondary asteroid and the granular materials enveloping the ejecta ring. As the secondary absorbs mass from this ring, the impact events predominantly occur on its leading side. When the secondary is not in 1:1 spin-orbit resonance, these impacts create a net torque countering the rotation of the secondary. As mass is continuously transferred from the ring to the secondary, this process catalyzes a quick decrease in the secondary's rotation rate. Importantly, this outcome will materialize due to a substantial mass absorption, underscoring the potency of this mechanical process in influencing the final rotation state of the secondary entity.

This study bears notable implications and significance across various dimensions. Foremost, it furnishes theoretical underpinnings for estimating the rotation and orbital characteristics of BASs immediately post-formation. This aspect has far-

reaching consequences, aiding in the refinement of estimates pertaining to the onset time of influential mechanisms such as tidal and thermal forces and developments of a comprehensive spin-orbit profile of BASs. Furthermore, the study establishes constraints governing the evolution trajectory and formation environment within the rotational breakup theory. Lastly, the proposed novel mechanism for rotation reduction holds the potential to alleviate the conundrum surrounding the prevalence of a sizable 1:1 spin-orbit resonant BAS population. These insights collectively contribute to the enhancement of our understanding of the distinctive properties of binary asteroids.

However, it is pertinent to acknowledge the study's limitations. The approach predominantly adopts minimalistic modeling considerations, involving assumptions such as a planar sphere-spheroid model. Additionally, aspects like the system's inclination, obliquity, and axis tilt of the seeds have been omitted. While these simplifications notably facilitate calculations while preserving correspondence with observations, employing more intricate models would undoubtedly offer deeper insights into the dynamics characterizing BASs and their formation. Furthermore, the descriptions related to seed migration are grounded in a mildly collisional environment, yet the prevalence of such environment needs further validation.

DECLARATION OF COMPETING INTEREST

The authors declare that they have no known competing financial interests or personal relationships that could have appeared to influence the work reported in this paper.

DATA AVAILABILITY

Data will be made available on request.

ACKNOWLEDGMENTS

This work is supported by the NASA/Solar System Exploration Research Virtual Institute (SSERVI), The Institute for Modeling Plasma, Atmospheres and Cosmic Dust (IMPACT).

REFERENCES

Blum, J., Schräpler, R., 2004. Structure and Mechanical Properties of High-Porosity Macroscopic Agglomerates Formed by Random Ballistic Deposition. Physical Review Letters 93, 115503. URL: https://link.aps.org/doi/10.1103/PhysRevLett.93.115503, doi:https://doi.org/10.1103/PhysRevLett.93.115503.

Bodrova, A., Schmidt, J., Spahn, F., Brilliantov, N., 2012. Adhesion and collisional release of particles in dense planetary rings. Icarus 218, 60–68. URL: https://linkinghub.elsevier.com/retrieve/pii/S0019103511004386, doi:https://doi.org/10.1016/j.icarus.2011.11.011.

Bottke, W.F., Vokrouhlický, D., Rubincam, D.P., Nesvorný, D., 2006. THE YARKOVSKY AND YORP EFFECTS: Implications for Asteroid Dynamics. Annual Review of Earth and Planetary Sciences 34, 157–191. URL: https://www.annualreviews.org/doi/10.1146/annurev.earth.34.031405.125154, doi:https://doi.org/10.1146/annurev.earth.34.031405.125154.

Brouwer, D., Clemence, G.M., 2014. Methods of Celestial Mechanics. Elsevier Science, Saint Louis. OCLC: 1058391593.

Dmitrašinović, V., 2020. Classical dynamics of three-body systems in the Efimov potential. Physical Review A 101, 053605. URL: https://link.aps.org/doi/10.1103/PhysRevA.101.053605, doi:https://doi.org/10.1103/PhysRevA.101.053605.

Goldreich, P., Sari, R., 2009. TIDAL EVOLUTION OF RUBBLE PILES. The Astrophysical Journal 691, 54–60. URL: https://iopscience.iop.org/article/10.1088/0004-637X/691/1/54, doi:https://doi.org/10.1088/0004-637X/691/1/54.

Hofmeister, A.M., Criss, R.E., Criss, E.M., 2018. Verified solutions for the gravitational attraction to an oblate spheroid: Implications for planet mass and satellite orbits. Planetary and Space Science 152, 68–81. URL: https://linkinghub.elsevier.com/retrieve/pii/S003206331730257X, doi:https://doi.org/10.1016/j.pss.2018.01.005.

Hyodo, R., Sugiura, K., 2022. Formation of Moons and Equatorial Ridge around Top-shaped Asteroids after Surface Landslide. The Astrophysical Journal Letters 937, L36. URL: https://iopscience.iop.org/article/10.3847/2041-8213/ac922d, doi:https://doi.org/10.3847/2041-8213/ac922d.

[Internet], T.F.D., 2003. MacCullagh's formula. URL: https://encyclopedia2.thefreedictionary.com/MacCullagh%27s+formula.

Jacobson, S.A., Scheeres, D.J., 2011. Dynamics of rotationally fissioned asteroids: Source of observed small asteroid systems. Icarus 214, 161–178. URL: https://linkinghub.elsevier.com/retrieve/pii/S0019103511001448, doi:https://doi.org/10.1016/j.icarus.2011.04.009.

Jacobson, S.A., Scheeres, D.J., McMahon, J., 2013. Formation of the wide asynchronous binary asteroid population. The Astrophysical Journal 780, 60. URL: https://iopscience.iop.org/article/10.1088/0004-637X/780/1/60, doi:https://doi.org/10.1088/0004-637X/780/1/60.

Johnston, R., 2022. Asteroids with Satellites. URL: http://www.johnstonsarchive.net/astro/asteroidmoons.html.

Muller, J.M., 1986. Sundman's inequality and zero velocity hypersurfaces in the general N-body problem. Astronomy and Astrophysics 155, L1. URL: https://ui.adsabs.harvard.edu/abs/1986A&A...155L...1M. aDS Bibcode: 1986A&A...155L...1M.

Murray, C.D., Dermott, S.F., 1999. Solar system dynamics. Cambridge University Press. URL: https://ui.adsabs.harvard.edu/abs/1999ssd..book.....M. publication Title: Solar system dynamics by C.D. Murray and S.F. McDermott. (Cambridge ADS Bibcode: 1999ssd..book.....M).

Pravec, P., Scheirich, P., Kušnirák, P., Hornoch, K., Galád, A., Naidu, S., Pray, D., Világi, J., Gajdoš, , Kornoš, L., Krugly, Y., Cooney, W., Gross, J., Terrell, D., Gaftonyuk, N., Pollock, J., Husárik, M., Chiorny, V., Stephens, R., Durkee, R., Reddy, V., Dyvig, R., Vraštil, J., Žižka, J., Mottola, S., Hellmich, S., Oey, J., Benishek, V., Kryszczyńska, A., Higgins, D., Ries, J., Marchis, F., Baek, M., Macomber, B., Inasaridze, R., Kvaratskhelia, O., Ayvazian, V., Rumyantsev, V., Masi, G., Colas, F., Lecacheux, J., Montaigut, R., Leroy, A., Brown, P., Krzeminski, Z., Molotov, I., Reichart, D., Haislip, J., LaCluyze, A., 2016. Binary asteroid population. 3. Secondary rotations and elongations. Icarus 267, 267–295. URL: https://linkinghub.elsevier.com/retrieve/pii/S0019103515005722, doi:https://doi.org/10.1016/j.icarus.2015.12.019.

Scheeres, D.J., 2002. Stability in the Full Two-Body Problem, in: Celletti, A., Ferraz-Mello, S., Henrard, J. (Eds.), Modern Celestial Mechanics: From Theory to Applications. Springer Netherlands, Dordrecht, pp. 155–169. URL: http://link.springer.com/10.1007/978-94-017-2304-6_10, doi:https://doi.org/10.1007/978-94-017-2304-6$_1$0.

Scheeres, D.J., 2004. Bounds on Rotation Periods of Disrupted Binaries in the Full 2-Body Problem. Celestial Mechanics and Dynamical Astronomy 89, 127–140. URL: http://link.springer.com/10.1023/B:CELE.0000034503.44164.b5, doi:https://doi.org/10.1023/B:CELE.0000034503.44164.b5.

Scheeres, D.J., 2009. Stability of the planar full 2-body problem. Celestial Mechanics and Dynamical Astronomy 104, 103–128. URL: http://link.springer.com/10.1007/s10569-009-9184-7, doi:https://doi.org/10.1007/s10569-009-9184-7.

Steinberg, E., Sari, R., 2011. Binary YORP and Evolution of Binary Asteroids. The Astronomical Journal 141, 55. URL: http://arxiv.org/abs/1010.2676, doi:https://doi.org/10.1088/0004-6256/141/2/55. arXiv:1010.2676 [astro-ph].

Walsh, K., Richardson, D., 2006. Binary near-Earth asteroid formation: Rubble pile model of tidal disruptions. Icarus 180, 201–216. URL: https://linkinghub.elsevier.com/retrieve/pii/S0019103505003210, doi:https://doi.org/10.1016/j.icarus.2005.08.015.

Walsh, K.J., Ballouz, R.L., Jawin, E.R., Avdellidou, C., Barnouin, O.S., Bennett, C.A., Bierhaus, E.B., Bos, B.J., Cambioni, S., Connolly, H.C., Delbo, M., DellaGiustina, D.N., DeMartini, J., Emery, J.P., Golish, D.R., Haas, P.C., Hergenrother, C.W., Ma, H., Michel, P., Nolan, M.C., Olds, R., Rozitis, B., Richardson, D.C., Rizk, B., Ryan, A.J., Sánchez, P., Scheeres, D.J., Schwartz, S.R., Selznick, S.H., Zhang, Y., Lauretta, D.S., 2022. Near-zero cohesion and loose packing of Bennu's near subsurface revealed by spacecraft contact. Science Advances 8, eabm6229. URL: https://www.science.org/doi/10.1126/sciadv.abm6229, doi:https://doi.org/10.1126/sciadv.abm6229.

Walsh, K.J., Richardson, D.C., Michel, P., 2008. Rotational breakup as the origin of small binary asteroids. Nature 454, 188–191. URL: http://www.nature.com/articles/nature07078, doi:https://doi.org/10.1038/nature07078.

Ćuk, M., 2007. Formation and Destruction of Small Binary Asteroids. The Astrophysical Journal 659, L57–L60. URL: https://iopscience.iop.org/article/10.1086/516572, doi:https://doi.org/10.1086/516572.